Preprints of the 18th IFAC World Congress
Milano (Italy) August 28 - September 2, 2011

Interplay between Feedback and Feedforward Control in Fly Gaze Stabilization

Daniel A. Schwyn [*] **Francisco J. H. Heras** [*,**]
Gino Bolliger [*,***] **Matthew M. Parsons** [*]
Holger G. Krapp [*] **Reiko J. Tanaka** [*,****]

[*] *Department of Bioengineering, Imperial College London, London SW7 2AZ, UK (e-mail: r.tanaka@imperial.ac.uk)*
[**] *Département de Mathématiques, Université Montpellier 2, 34095 Montpellier cedex 5, France*
[***] *Institute for Biomedical Engineering, ETH Zurich, 8092 Zurich, Switzerland*
[****] *Institute for Mathematical Sciences, Imperial College London*

Abstract: Flies rely on a powerful gaze stabilization reflex to facilitate visual control and guidance of flight. We performed behavioral experiments and systems identification to study the contribution of two major sensory systems to gaze stabilization: the mechanosensory halteres, and the compound eyes. We measured the frequency response of compensatory head roll induced by forced thorax movements with and without halteres. Based on a simplified, linear architecture, we derived transfer functions for the two sensory pathways and the neck motor system that actuates changes of head position. The resulting bandwidths and response delays were consistent with data from the literature.

Keywords: Biocybernetics, closed-loop control, system identification

1. INTRODUCTION

Flies are recognized as a successful model system to study flight control (Taylor and Krapp [2007]). They achieve a remarkable aerial manoeuvrability when performing a limited repertoire of behaviours and reflexes, all controlled by a comparatively simple nervous system. The variety of distributed sensors contributing to feedback and feedforward pathways in flies is a prominent example of dynamic range fractioning and multi-sensory integration typically found in biological and bio-inspired control systems (Frye [2010]).

Appropriate use of visual information for flight control requires insects, in general, to maintain a level orientation of their eyes, and therefore their head. This ensures the visual scene is kept at a default orientation during locomotion and mitigates the problem of image blur, when rapid movements result in visual motion exceeding the bandwidth of the visual system (van Hateren [1999]). In order to achieve this goal, the fly's gaze is controlled by a powerful stabilization reflex (Hengstenberg [1993]) that is driven by inputs from a variety of sensory modalities. Visual and mechanosensory cues enable the insect to keep its gaze stable even if its body experiences considerable attitude changes.

In previous studies, Hengstenberg and colleagues (Hengstenberg *et al.* [1986], Hengstenberg [1991]) investigated the dynamics of the fly's head roll responses mediated by different sensory organs using varying stimulus time courses (sinusoids, step functions and others). They concluded that information from several sensory systems covering different but partially overlapping fractions of the dynamic input range are integrated to obtain reliable control signals, but stopped short of formal descriptions and models of the gaze stabilization system. In a recent study, Huston and Krapp [2009] further examined the fusion of visual and mechanosensory inputs. Their results suggest that information is combined at the level of the neck motor neurons in a non-linear fashion rather than by a simple, weighted addition. However, at the behavioral level, there is evidence that information from different sensory modalities is aggregated in a nearly linear fashion (Hengstenberg [1993]). The muscular apparatus responding to the resulting signal has been described anatomically in Strausfeld *et al.* [1987] and Gilbert *et al.* [1995], but its biomechanical simulation is not yet possible due to a lack of physiological information.

This paper is concerned with the interplay of feedback and feedforward pathways provided by distinctly different sensor systems with complementary dynamic characteristics that affects the overall closed-loop behavior and stability of the system. A combination of bio-inspired modeling and carefully designed experiments that are amenable to control theoretical analysis enabled us to systematically tackle this complex problem (see Graetzel *et al.* [2010], and Barron and Srinivasan [2006] for other examples of behavioral identification of biological systems). We tried to keep our experimental and theoretical frameworks as simple as possible in an attempt to only capture the essential functional features of the fly gaze control system.

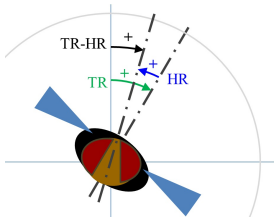

Fig. 1. Definition of input signal (TR) and output signal (HR) of the gaze stabilization system. Note the direction of HR.

We developed a linear model with one actuator, the neck motor system, driven by a linear combination of visual feedback and mechanosensory feedforward sensor signals. Using the experimental data of head roll responses triggered by externally induced thorax oscillations at different frequencies, we identified a possible set of transfer functions for the sensors and the actuator, and suggest a putative control architecture of the system. We then verified that our model under closed-loop simulation conditions successfully reproduced (i) the main functional features of the fly gaze stabilization system and (ii) experimental data previously reported in the literature.

This paper is organized as follows: Section 2 introduces the model structure with particular emphasis on simplifying assumptions. Section 3 describes the experimental methods and conditions we used to obtain the closed-loop frequency responses of the system. In Section 4, we carry out the systems identification while Section 5 discusses the accuracy and scope of the identified model.

2. MODEL OVERVIEW

We developed a simple, linear control architecture for gaze control in the fly. We choose the thorax roll angle (TR) as the system's input and the head roll angle (HR) relative to TR as output (see Fig. 1). Note that, while TR is clockwise positive, HR is of positive sign for counterclockwise angles. Therefore, the total head deflection relative to the laboratory frame is TR-HR. Although compensatory head movements encompass rotations around all three axes, we limit ourselves to the study of head rotations around the animal's longitudinal axis, which have the largest amplitude (van Hateren [1999]). This allows us to describe the model as a single input single output (SISO) system and greatly simplifies our formalism.

We consider the control of head position to be based on the outputs of two major sensors, compound eyes and halteres, as well as one actuator, the neck motor system. Compound eyes (CEs) are rigidly attached to the head of the fly and consist of a large number of facets that process visual motion information. As they analyse relative motion between the eyes and the visual surroundings we assume the input to the compound eyes to be the angular velocity of the fly's head. Halteres (Hs) are small, club-shaped organs on the fly's thorax. They move in anti-phase to the wingbeat and are thought to measure the coriolis forces induced by rotations of the fly around its body axes (Nalbach [1994]). The neck motor system receives information from both CEs and Hs at the level of the neck motor neurons and interfaces a complex muscular apparatus that finally actuates head position.

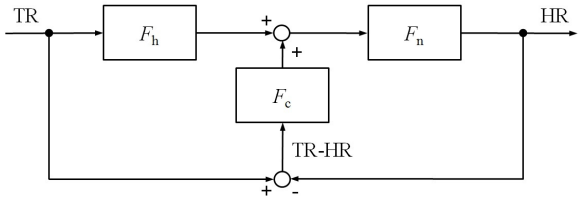

Fig. 2. Block diagram of the simplified gaze control system

The model structure presented in Fig. 2 is based on these subsystems. A similar structure has been independently proposed by Hengstenberg [1993]. The transfer functions corresponding to CEs, Hs and the neck motor system are $F_c(s)$, $F_h(s)$, and $F_n(s)$, respectively. Note that we use angular position rather than velocity for HR and TR by conventions used in the literature on lift responses in the fruit fly (Tanaka and Kawachi [2006], Graetzel *et al.* [2010]), although both angular position and angular velocity would be biologically plausible and mathematically equivalent choices.

As the CEs are attached to the fly's head, the input to F_c is the head deflection (TR-HR). Hs are located on the fly's thorax; the input to F_h is simply TR. Our model assumes the integration of information from CEs and Hs to be a linear sum for the sake of simplicity, that is, the input to F_n is the linear sum of the outputs of F_c and F_h. Although the multi-sensory integration at the level of neck motor neurons in reality is not as straightforward (Huston and Krapp [2009]), simulations in subsection 4.1 reveal that a linear model sufficiently captures the characteristics of this integration at the behavioral level.

The block diagram (Fig. 2) suggests that gaze stabilization is achieved by a well-balanced combination of feedback control by the CEs and feedforward control through the Hs. The CEs provide feedback on the error signal, which is defined as the deviation of the head from the horizontal. Moreover, it is known that CEs, Hs, and the neck motor system have different time delays (Taylor and Krapp [2007], Sandeman [1980]). The interplay among these differently tuned components is key to understanding the control principles underlying gaze stabilization. Our approach here is to identify a possible set of transfer functions for F_c, F_h, and F_n using the data from our carefully designed experiments, a more detailed account of which is provided in the next section.

3. EXPERIMENTS AND DATA

While white noise has sometimes been employed for the identification of LTI systems, for biological systems it is often preferred to sweep through a range of frequencies, as the results can be interpreted more easily and nonlinearities are readily eliminated from the analysis. We chose to drive the system by externally rotating the thorax and measured the time course of HR. The choice of input and output signals is not only crucial to the biological plausibility of the system; a clever choice also facilitates the extraction of a linear model.

We used the set-up shown in Fig. 3a to sample the TR-to-HR frequency responses of five female flies (*Calliphora vicina* from laboratory stock, aged between 5 and 10 days).

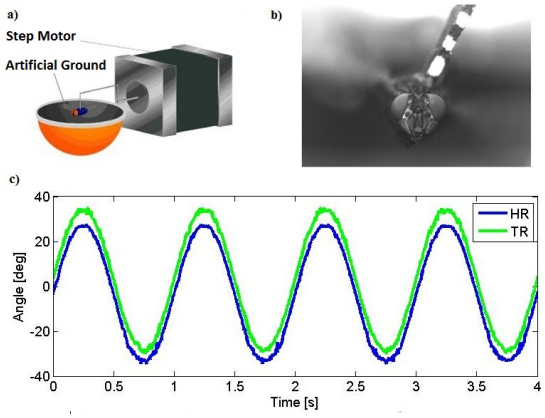

Fig. 3. a) Experimental set-up (adapted from Parsons [2008]), b) Sample frame of the high-speed video recording, c) Part of a sample time course of measured head roll and thorax roll

We first occluded the animal's ocelli, another visual sensor mediating information on the coarse distribution of light intensities in the visual field. The fly was then attached to a step motor which allowed its thorax to be rotated around the longitudinal (roll) axis, thereby driving the system's input. A dark-colored hemisphere was fixed below the fly, as an artificial ground that provides visual information to the CEs. This set-up is described in more detail by Parsons [2008].

We used frontal airflow to induce flight. During tethered flight, the flies were oscillated by $\pm 30°$ at 11 logarithmically spaced frequencies between 0.01 and 15 Hz for at least 10 cycles per frequency/trial. The motor was controlled with a custom-written LabVIEW2009 program (National Instruments, Austin, TX). The resulting head movements of the fly were recorded using a Fastcam SA3 high speed camera (Photron, San Diego, CA). The frame rate of the camera was increased with stimulation frequency to acquire a sufficient number of frames per cycle in all trials.

These experiments were repeated for two different sensory conditions. In the first condition (C1), only the fly's ocelli were disabled while CEs and Hs were left intact. In the second condition (C2), the Hs were surgically removed, in addition to the occlusion of the ocelli, so that the CEs are the only major sensors in this condition. As the coriolis forces measured by the Hs depend on the inertial moment of these stalks (Nalbach and Hengstenberg [1986]), their removal is assumed to eliminate all haltere-mediated information.

The resulting image sequences (Fig. 3b) were processed semi-automatically to extract the time course of thorax roll (TR) and head deflection (TR-HR) in the laboratory frame (Fig. 3c). The gain and phase of both the input (TR) and output (HR) of the system at each TR frequency and for each condition were obtained from the respective Fourier spectra of the signals. In all of our experimental trials, the output's amplitude spectrum showed a strong peak at the input frequency ω_k (see also Subsection 4.1). Accordingly, the system gain was calculated for each input frequency ω_k as the ratio of the input and output amplitudes, $|\mathrm{HR}|_{\omega_k}/|\mathrm{TR}|_{\omega_k}$. Similarly, the phase ϕ_{ω_k} was

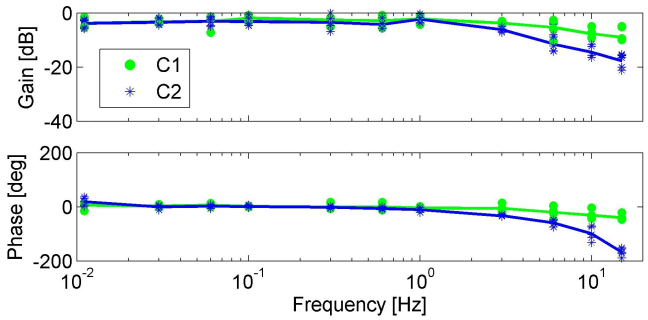

Fig. 4. Experimental data for conditions C1 and C2, responses of individual flies (dots/stars) and averages across flies (solid lines)

defined as the phase difference between input and output spectra at the input frequency ω_k.

The resulting bode plots are shown in Fig. 4. Both gain and phase vary smoothly across the frequency range under investigation. For both conditions, the gain is close to one for frequencies up to 1 Hz. The phase in this range is close to 0°, representing perfect compensation. For higher oscillation frequencies, the gain falls and the response becomes significantly delayed, as indicated by a rapidly decreasing phase. The decreases in gain and phase are particularly pronounced in C2 (only CEs) compared to C1 (Hs and CEs). Due to the considerable variability of responses between flies, particularly at higher frequencies, we decided to use the average gain and phase of the flies and investigated the average system rather than an ensemble of transfer functions (one transfer function per fly).

4. CHARACTERIZATION OF SUBSYSTEMS

4.1 Assessment of linearity

The behavior of an LTI system is fully characterized by its transfer function. As many biological (sub-)systems exhibit highly non-linear behaviors, the prerequisite of linearity should be verified explicitly (Graetzel *et al.* [2010]). We tested two properties that have to be met by linear systems, (1) superposition and (2) sinusoidal fidelity. Sinusoidal fidelity means that, if a linear system is driven by a pure sinusoid, the output will be a pure sinusoid at the same frequency. This does not preclude a change in either phase or amplitude.

We used the experimental set-up described in Section 3 to provide a TR stimulus that consisted of a combination of oscillations at the two frequencies $f_1 = 4$ Hz and $f_2 = 5$ Hz. We recorded HR in response to this stimulus in 4 female flies with both Hs and CEs intact. For a linear system, we would expect the output HR to only include components at the stimulation frequencies f_1 and f_2. Indeed, the Fourier spectrum of HR (Fig. 5) is dominated by peaks at f_1 and f_2. Higher-order harmonics are of much lower amplitude. We calculated the ratio of the second-order harmonics to the fundamental as $\mathrm{IMD}_2 = \frac{E(f_1+f_2)}{E(f_2)} = \frac{E(9Hz)}{E(5Hz)}$, where $E(f)$ is the energy spectral density of HR at frequency f. We find that the average second-order IMD across the four flies varies be-

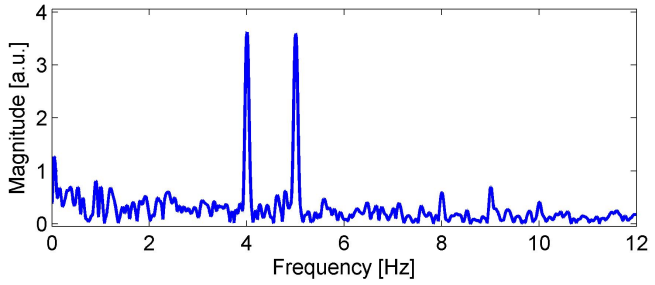

Fig. 5. FFT of the response of a single fly to the superposition of TR frequencies $f_1 = 4$ Hz and $f_2 = 5$ Hz

tween 2% and 4%. Analoguosly, we calculated the third-order IMD ratio to lie in the range between 2% and 3% for the four flies. We repeated the same experiments with (1) another combination of frequencies (4.5 and 4.8 Hz) and (2) after removal of the halteres. In both cases, we found IMD values in the above range. This confirms that the system's input-output relationship can be reasonably assumed to be linear, although we would need to show that the system meets both the superposition and homogeneity requirements to prove its linearity. As we expect saturation to occur at larger angles, we limited both our experiments and the model to amplitudes not higher than 30°.

4.2 Identification of subsystem transfer functions

Using the data obtained in the form of bode plots in Fig. 4, we identify a possible set of transfer functions for $F_{\rm c}(s), F_{\rm h}(s)$, and $F_{\rm n}(s)$, such that the closed-loop behavior of our model captures the salient characteristics of the experimental data.

Let $G_1(s)$ and $G_2(s)$ denote the closed-loop transfer functions for the conditions C1 and C2, respectively. They are described in terms of $F_{\rm c}(s), F_{\rm h}(s)$, and $F_{\rm n}(s)$ by

$$G_1(s) = \frac{F_{\rm n}(s)(F_{\rm c}(s) + F_{\rm h}(s))}{F_{\rm n}(s)F_{\rm c}(s) - 1} \tag{1}$$

and

$$G_2(s) = \frac{F_{\rm n}(s)F_{\rm c}(s)}{F_{\rm n}(s)F_{\rm c}(s) - 1}, \tag{2}$$

respectively, as is seen from the block diagram in Fig. 2.

Thus we first identify

$$G(s) := \frac{F_{\rm h}(s)}{F_{\rm c}(s)} = \frac{G_1(s)}{G_2(s)} - 1, \tag{3}$$

which is independent of $F_{\rm n}(s)$.

Let $\{\hat{G}_1(\omega_k)\}_{k=1}^{11}$ and $\{\hat{G}_2(\omega_k)\}_{k=1}^{11}$ denote the data (a pair of gain and phase at each frequency) for the conditions C1 and C2, respectively. Using $\{\hat{G}_1(\omega_k)\}$ and $\{\hat{G}_2(\omega_k)\}$, we prepare the bode plot $\{\hat{G}(\omega_k)\}$ corresponding to $G(s)$ in (3), for which we identify the transfer function $\tilde{G}(s) = \frac{\tilde{F}_{\rm h}(s)}{\tilde{F}_{\rm c}(s)}$ (Fig. 6). The bode plot of $\{\hat{G}(\omega_k)\}$ suggests that there is a single zero around 1 Hz (slope of +20dB per decade in the range of the four highest frequencies). As it is unlikely that either $F_{\rm h}$ or $F_{\rm c}$ are purely proportional controllers, and in order to increase the flexibility of the fitting procedure, we added a pole and a further zero. We therefore assume that both $\tilde{F}_{\rm c}(s)$ and $\tilde{F}_{\rm h}(s)$ are described by rational transfer functions with gains $K_{\rm c}$ and $K_{\rm h}$ and delay terms $\tau_{\rm c}$ and $\tau_{\rm h}$, respectively,

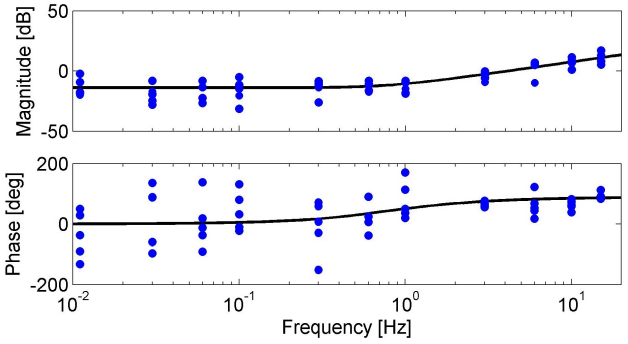

Fig. 6. Bode plot for $\{\hat{G}(\omega_k)\}$ and the fitted function $\tilde{G}(s)$

and further assume that $\tilde{G}(s)$ has two zeros, z_1 and z_2, and one pole p, i.e.

$$\tilde{G}(s) = K\frac{(s - z_1)(s - z_2)}{(s - p)}e^{-s\Delta\tau},$$

where $K = K_{\rm h}/K_{\rm c}$ and $\Delta\tau = \tau_{\rm h} - \tau_{\rm c}$.

The first step in identifying $\tilde{G}(s)$ is to estimate the delay term. We obtain $\Delta\tau = 9.1 \times 10^{-3}$ [sec] by applying the formula

$$\Delta\tau = -\frac{1}{k_p - k_l}\sum_{k=k_p}^{k_l-1}\frac{\arg(G(j\omega_{k+1})) - \arg(G(j\omega_k))}{\omega_{k+1} - \omega_k} \tag{4}$$

(Pintelon and Schoukens [2001]) to the phase data of the five highest frequencies ω_i $(i = 7, \ldots, 11)$, a frequency range where the variability is low and we do not expect any poles or zeros (no apparent corner frequencies in the gain plot). Other means of estimating the delay term, e.g. deducting the contribution of the poles and zeros from the phase, resulted in similar delay values ($\Delta\tau = 9.4 \times 10^{-3}$ [sec]).

We then obtain the least-squares fit of $\tilde{G}(j\omega_k)$ to the gain plot of $\{\hat{G}(\omega_k)\}$ using `fminsearch` (implementing the Nelder-Mead method) in Matlab. The phase plot exhibits too high a variance to reasonably perform a fit.

These two fitting steps result in

$$\tilde{G}(s) = 0.0377\frac{(s + 3.741)^2}{s + 2.586}e^{s(9.1*10^{-3})}. \tag{5}$$

We distribute the poles and zeros of $\tilde{G}(s)$ between $\tilde{F}_{\rm c}(s)$ and $\tilde{F}_{\rm h}(s)$ based on our biological knowledge (Hengstenberg [1993]) that the compound eyes $(F_{\rm c}(s))$ act as a bandpass filter for intermediate frequencies while halteres $(F_{\rm h}(s))$ behave like a highpass filter, and obtain

$$\tilde{F}_{\rm c}(s) = K_{\rm c}\frac{s}{(s + 3.741)^2}e^{-s(\tau_{\rm h}+9.1\times10^{-3})} \tag{6}$$

and

$$\tilde{F}_{\rm h}(s) = 0.0377K_{\rm c}\frac{s}{s + 2.586}e^{-s\tau_{\rm h}}, \tag{7}$$

where $K_{\rm c}$ is a free parameter. Note that we introduce a derivative (s) term in both transfer functions as we expect both sensory modalities to respond to angular velocities rather than angular position. The delay in the haltere pathway is set to be $\tau_{\rm h} = 5 \times 10^{-3}$ [sec] (Taylor and Krapp [2007]), resulting in $\tau_{\rm c} = \tau_{\rm h} - \Delta\tau = 14.1 \times 10^{-3}$ [sec].

It is straightforward to see from (1) and (2) that $F_{\rm n}(s)$ is described as $F_{\rm n1}(s) := -\frac{1}{F_{\rm c}(s)}\frac{G_2(s)}{1+G_2(s)}$ as well as

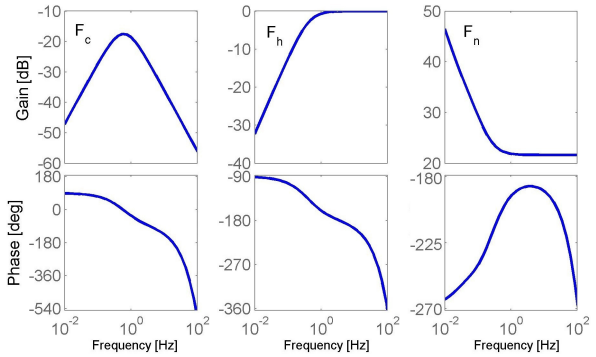

Fig. 7. Identified transfer functions for $F_{\rm c}, F_{\rm h}$ and $F_{\rm n}$

$F_{\rm n2}(s) := -\frac{1}{F_{\rm h}(s)}\frac{G_1(s)-G_2(s)}{1+G_2(s)}$. Using $\{\hat{G}_1(\omega_k)\}$, $\{\hat{G}_2(\omega_k)\}$, $\tilde{F}_{\rm c}(s)$ in (6), and $\tilde{F}_{\rm h}(s)$ in (7), we prepare the bode plot $\{\hat{F}_{\rm n1}(\omega_k)\}$ and $\{\hat{F}_{\rm n2}(\omega_k)\}$ corresponding to $F_{\rm n1}(s)$ and $F_{\rm n2}(s)$, respectively. As $\{\hat{F}_{\rm n1}(\omega_k)\}$ and $\{\hat{F}_{\rm n2}(\omega_k)\}$ turn out to be very similar, we take their mean at each frequency to obtain $\{\hat{F}_{\rm n}(\omega_k)\}$, for which we fit a transfer function $\tilde{F}_{\rm n}(s)$. We assume that $\tilde{F}_{\rm n}(s)$ is described by a rational transfer function with delay term $\tau_{\rm n}$ and further assume that $\tilde{F}_{\rm n}(s)$ has one zero and one pole, which is at zero to cancel out the s term in both, $\tilde{F}_{\rm c}(s)$ and $\tilde{F}_{\rm h}(s)$. It can also be argued that the neck motor system should behave like an integrator for the sake of biological plausibility.

We first obtain $\tau_{\rm n} = 5.11 \times 10^{-3}$ [sec] in the same way as we did for $\Delta\tau$, using the phase data at the four highest frequencies ω_i $(i = 8, \ldots, 11)$. We then obtain the least-squares fit of $\tilde{F}_{\rm n}(s)$ using the gain and phase data for $\{\hat{F}_{\rm n}(\omega_k)\}$ via `fminsearch` in Matlab, resulting in

$$\tilde{F}_{\rm n}(s) = -\frac{1}{K_{\rm c}} 12.520 \frac{(s+1.745)}{s} e^{-s(5.110\times10^{-3})}. \quad (8)$$

Note that the distribution of constant gains and delays between motor system, $F_{\rm n}(s)$, and sensory modalities, $F_{\rm c}(s)$ and $F_{\rm h}(s)$, is not unique in our model. All such combinations are mathematically equivalent and will not influence the closed-loop behavior of our model. The free parameter $K_{\rm c}$ represents the constant gain distribution. Our result also shows that the delays can be distributed under the constraint that $\tau_{\rm h} + \tau_{\rm n} = 10.11 \times 10^{-3}$ [sec], which is consistent with latencies reported in the literaure (Hengstenberg [1993]).

The identified transfer functions (Fig. 7) provide clues regarding the control principles underlying gaze stabilization, especially on the coordination of sensory modalities. Compound eyes and halteres seem to be responsible for feedback and feedforward control, respectively (see Fig. 2). Above analysis suggests that the halteres have a much smaller time delay and a much smaller gain compared to the compound eyes ($\tau_{\rm c} - \tau_{\rm h} = 9.1 \times 10^{-3}$ [sec] and $K_{\rm h}/K_{\rm c} = 0.0377$). Rapid, mechanosensory feedforward control sets in first after the thorax rotates. It ensures an approximate compensation of the thorax movement. The compensation error then triggers slower feedback control via the compound eyes. This is consistent with the fact that visual information plays an important role in flight control and is assisted by the information obtained from other sensors.

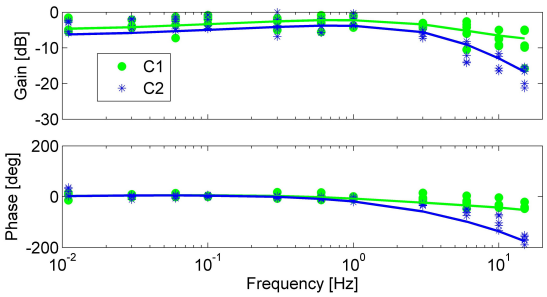

Fig. 8. Bode plot for the model ($\tilde{G}_1(s)$ and $\tilde{G}_2(s)$, solid lines) and original data (dots/stars)

4.3 Closed-loop behavior of our model

The bode plot of the closed-loop transfer functions $\tilde{G}_1(s)$ and $\tilde{G}_2(s)$ (for conditions C1 and C2, respectively) obtained by replacing $F_{\rm c}(s)$, $F_{\rm h}(s)$, and $F_{\rm n}(s)$ in the right hand sides of (1) and (2) by the fitted transfer functions (5), (6), and (7), respectively, is shown in Fig. 8. There is a close match between the measured data and our model for both gain and phase. Fitting a delay term to the phase of the bode plots in Fig. 8 estimates behavioral latencies to be 9 [ms] for C1 and 33 [ms] for C2. This is in good agreement with the behavioral latencies of 10 [ms] and 30 [ms] reported in Hengstenberg [1993] in the corresponding conditions.

In order to verify that our mathematical model faithfully replicates experimentally determined stimulus-response relationships, we implemented the closed-loop system with the fitted transfer functions in Matlab Simulink v.7.2. The delay terms were approximated using the 5th order Padé approximation and we chose a constant stepsize of 0.5 [ms]. We were able to reproduce the experimental results in Hengstenberg *et al.* [1986] where a sinusoidal stimulus with ± 90° amplitude is used. In this case, the gain in our model is slightly higher than the gain found in the literature (0.75 in our model rather than 0.7). This is in intuitive agreement with the expected saturation of the neck motor system at high amplitudes. This simulation platform will serve as a tool to investigate the functional organization of the gaze stabilization reflex in the fly and to predict the outcomes of future experiments.

5. CONCLUSION

This paper describes the first step of our ultimate goal to establish a closed-loop simulation platform to study the functional properties, performance limits and the way in which signals from different modalities are integrated in the fly gaze control system. Using systems identification methods, we investigated the interplay of feedback and feedforward pathways realized by two major sensors with complementary dynamic characteristics and revealed some of the essential control principles employed by this system.

We assumed a simplified, linear control design ("grey box") of the gaze control system, and derived a set of sensor and actuator transfer functions using experimental data in the form of the frequency responses of head roll induced by thorax rotation in flies after disabling subsets of sensory organs. Simulations using these transfer func-

tions faithfully reproduced the experimental results and many characteristics found in the literature. The control system structure and identified subsystem transfer functions readily suggest that sophisticated gaze stabilization is realized in part by a well-balanced combination of a fast mechanosensory feedforward controller with smaller gain, and a slower feedback controller with higher gain. These two control mechanisms ensure a quick approximate compensation via mechanosensory sensors followed by slow but more precise compensation of thorax movement. In our model, the compound eyes are described by a bandpass filter tuned to intermediate frequencies, while the halteres are described by a highpass filter. They could reproduce the overall system behavior, although the real halteres would obviously saturate at very high frequencies.

It is remarkable that a biological control system such as the gaze stabilization system, made up of numerous nonlinear processes, exhibits the high linearity that we observed here (Fig. 5). It allowed us to reasonably use a linear model with appropriate choice of system inputs and outputs. This highly simplified system enabled us to capture important features of the gaze control system's dynamics. In our block diagram (Fig. 2), we could successfully separate feedforward and feedback branches to facilitate a simple analysis without explicitly considering voluntary manoeuvres. This was possible because we stimulated the flies through forced thorax roll, which simulates a turbulence caused by a gust of wind rather than a voluntary movement, such as a saccade. This generic 2-DoF controller configuration has been extensively studied (Araki and Taguchi [2003]) and is known to perform well at reference tracking and disturbance rejection. Such theoretical knowledge may aid a more detailed analysis of the stability and robustness of the fly gaze stabilisation system. To investigate the limits of our linear model, we will conduct further experiments varying the amplitude of the thorax oscillations and extend our computational analysis, for example to include a nonlinearity after the integration of the two sensory branches, as has been suggested by Huston and Krapp [2009].

Our future research will aim to further develop both modeling frameworks and experimental designs, and will include the following two directions: (1) analysis of additional sensors and (2) investigation of sensor dynamics. Future experiments may not only include the ocelli, but also the prosternal organs, head-neck posture sensors that play an active role in head-neck coordination and the correction of accumulating positional errors. The model we obtained will allow us to investigate the influence of modifications in the dynamics of individual sensory organs on the stability and accuracy of the reflex.

The results in this paper show that phenomenological grey box analysis is a promising approach to analyze biological control systems. The gaze stabilization reflex in flying insects employs principles relevant to artificial control and will serve as a basis for further studies on different aspects of flight and gaze control.

ACKNOWLEDGEMENTS

The authors would like to thank Karin Bierig for performing most of the behavioral experiments, and Shuichi Adahi and Hiroshi Oku for their comments on the manuscript. This study was supported by USAF grants FA8655-09-1-3022 and FA8655-09-1-3083 to HGK. RJT is supported by an EPSRC career acceleration fellowship.

REFERENCES

M. Araki and H. Taguchi. Two-Degree-Of-Freedom PID Controllers. *Int. J. Control. Autom.*, 4:401–411, 2003.

A. Barron and M.V. Srinivasan. Visual regulation of ground speed and headwind compensation in freely flying honey bees (*Apis mellifera L.*). *J. Exp. Biol.*, 209:987–984, 2006.

M.A. Frye. Multisensory systems integration for high-performance motor control in flies. *Current Opinion in Neurobiology*, 20:347–352, 2010.

C. Gilbert, W. Gronenberg, and N.J. Strausfeld. Oculomotor control in calliphorid flies: Head movements during activation and inhibition of neck motor neurons corroborate neuroanatomical predictions. *J. Comp. Neurology*, 361(2):285–297, 1995.

C.F. Graetzel, B.J. Nelson, and S.N. Fry. Frequency response of lift control in *Drosophila*. *J. R. Soc. Interface*, 7:1603–1616, 2010.

R. Hengstenberg, D.C. Sandemann, and B. Hengstenberg. Compensatory head roll in the blowfly during flight. *Proc. R. Soc. London B*, 277:455–482, 1986.

R. Hengstenberg. Gaze control in the blowfly *Calliphora*: a multisensory, two-stage integration process. *Seminars in the Neurosciences*, 3:19–29, 1991.

R. Hengstenberg. Multisensory control in insect oculomotor systems. In F.A. Miles, and J. Wallman, editors, *Visual Motion and its Role in the Stabilization of Gaze* 285–298. Elsevire Science Publishers B.V, 1993.

S.J. Huston and H.G. Krapp. Nonlinear Integration of Visual and Haltere Inputs in Fly Neck Motor Neurons. *J. Neurosci.*, 29(42):13097-13105, 2009.

G. Nalbach and R. Hengstenberg. Halteres of *Calliphora* - a sense organ for rotations. *Verh. Dtsch. Zool. Ges.*, 79:229, 1986.

G. Nalbach. Extremely non-orthogonal axes in a sense organ for rotation: behavioural analysis of the dipteran haltere system. *Neuroscience*, 61:155–163, 1994.

M.M. Parsons. *Multisensory Integration of Self-Motion Information in the Blowfly, Calliphora vicina.* PhD Thesis, University of Cambridge, 2008.

R. Pintelon and J. Schoukens. *System Identification: A Frequency Domain Approach.* IEEE Press, New York, 2001.

D.C. Sandemann. Head movements in flies (*Calliphora*) produced by deflexion of the halteres. *J. Exp. Biol.*, 85: 43–60, 1980.

N.J. Strausfeld, H.S. Seyan, and J.J. Milde. The neck motor system of the fly *Calliphora erythrocephala*. I . Muscles and motor neurons. *J. Comp. Physiol*, 160: 205–224, 1987.

K. Tanaka and K. Kawachi. Response characteristics of visual altitude control system in *Bombus terrestris J. Exp. Biol.*, 209:4533–4545, 2006.

G.K. Taylor and H.G. Krapp. Sensory systems and flight stability: What do insects measure and why? *Adv Insect Physiol*, 34:231–316, 2007.

J.H. van Hateren and C. Schilstra. Blowfly Flight and Optic Flow - II Head Movements during flight *J. Exp. Biol.*, 202:1491–1500, 1999.